Explaining the Dependences of the Hole and Electron Mobilities in Si Inversion Layers

Agostino Pirovano, *Student Member, IEEE*, Andrea L. Lacaita, *Senior Member, IEEE*, Günther Zandler, and Ralph Oberhuber

***Abstract*—In this work the hole surface roughness-limited mobility in Si MOSFET's is investigated. Based on full-band Monte Carlo simulations and on an equivalent relaxation-time numerical model, we show that the differences between hole and electron experimental mobilities are not due to any peculiar physics of the valence band. They can be instead accounted for by a suitable shape of the power spectrum describing the surface roughness. The new power spectrum explains the experimental dependences of both electron and hole mobilities using the same surface roughness parameters. Finally the spatial features of the roughness described by the new spectrum are discussed and compared to those represented by Gaussian and exponential auto-covariance functions.**

***Index Terms*—Charge carrier mobility, semiconductor-insulator interfaces, modeling, MOSFET's.**

I. INTRODUCTION

BEGINNING in the early 1960's, carrier mobility in silicon inversion layers has been extensively studied, and the dominant scattering mechanisms have been carefully investigated. It is well established that the mobility data fall on the so called *universal curves*, independent of the channel doping, when plotted as a function of the transverse effective field [1]:

$$E_{eff} = \frac{1}{\epsilon_{si}}(Q_d + \eta Q_{inv}) \tag{1}$$

where Q_d and Q_{inv} are the depletion and inversion charges, respectively, while η is an empirical coefficient tailored to optimize the alignment of the experimental data. From a physical standpoint the effective field is related to the electric field pushing the carriers against the Si/SiO_2 interface. The larger E_{eff}, the closer the carriers to the interface, the larger the mobility degradation due to surface roughness scattering.

However, the universal curves of electrons and holes feature some remarkable differences. First of all, the former is derived by plotting the mobility as a function of E_{eff} with $\eta = 1/2$, while the hole mobility data are universal by taking $\eta = 1/3$ [2]. Moreover, at low temperature and large effective fields, where surface scattering is dominant, the electron mobility degrades as E_{eff}^{-2} while the hole mobility follows an E_{eff}^{-1} power law. The aim of our work has been to clarify whether these differences are accidental, resulting from the superposition of many effects, or if instead they can be ascribed to a single physical reason.

Based on detailed calculations of the surface roughness-limited mobility, we show that modifying the shape of the roughness power spectrum (i.e., assuming a different auto-covariance function for the surface roughness at the Si/SiO_2 interface) the above dependences can be quantitatively explained. Since the surface roughness-limited mobility can be more reliably observed at low temperature, we will mainly refer to experimental data and simulation results at 77 K.

As pointed out in [3], the degeneracy between the heavy- and the light-hole bands close to the Γ point makes the $E(\mathbf{k})$ energy dispersion curves dependent on gate bias. Therefore, a detailed band structure calculation is needed, which has been obtained by self-consistently solving the one dimensional Poisson and Schrödinger equations with a six-band $\mathbf{k}\cdot\mathbf{p}$ procedure [5]. The corresponding $E(\mathbf{k})$ functions for the different subbands are then used by a momentum space full-band Monte Carlo code [4].

In order to get physical insight into the Monte Carlo results we have also used an equivalent effective mass model (Section II). Section III deals with the main features of the surface roughness scattering model implemented in the calculations. It also shows that the mobility computed at 77 K by assuming a single parabolic band favorably compares with the numerical results of the full-band Monte Carlo code. The more efficient relaxation-time model was therefore extensively used throughout the work. In Section IV the impact of the power spectrum on the carrier mobility is discussed. In Section V the power spectrum accounting for the experimental dependences is presented. A summary of the work is reported in Section VI.

II. VALENCE BAND STRUCTURE AND EQUIVALENT EFFECTIVE MASSES

Even if the silicon valence band structure is far from being isotropic and parabolic, it has been already shown [4] that the holes drift velocity and their average kinetic energy at room temperature can be accounted for by adopting a single parabolic band. In this section we describe the steps followed to identify a convenient parabolic band model at 77 K.

The quantization effective mass m_z in the direction orthogonal to the Si/SiO_2 interface has been extracted comparing the value of the lowest energy level E_0 of each subband (as obtained

Manuscript received March 12, 1999; revised September 7, 1999. This work was supported in part by the Italian Ministry of the University by The Italian National Research Council, and by Deutsche Forschungsgemeinschaft. The review of this paper was arranged by Editor K. Shenai.

A. Pirovano and A. L. Lacaita are with the Dipartimento di Elettronica e Informazione, Politecnico di Milano, I-20133 Milano, Italy (e-mail: lacaita@elet.polimi.it).

G. Zandler and R. Oberhuber are with the Physics Department and Walter Schottky Institute, Technical University of Munich, D-85748 Garching, Germany.

Publisher Item Identifier S 0018-9383(00)01949-3.

S0018-9383/00$10.00 © 2000 IEEE

from the $\mathbf{k}\cdot\mathbf{p}$ calculations) with the corresponding value given by the Airy formula [6], that is

$$E_0 = \left(\frac{\hbar^2}{2m_z}\right)^{1/3} \left[\frac{9\pi eF}{8}\right]^{2/3} \tag{2}$$

where F is the transverse electric field. We have taken for F the electric field at the centroid of the hole wave-function. Since the external field lifts the degeneracy of the valence bands at the Γ point, the band structure is field dependent. However, it turns out that the F dependence of the heavy-hole subband is weak. Its quantization effective mass can be safely taken equal to $0.275m_0$ up to $F = 1.0$ MV/cm. The light-hole subband is instead more sensitive, and the m_z value derived from (2) depends as:

$$m_z(F) = m_z(F_0) + A \times (F - F_0) \times m_0 \tag{3}$$

with $F_0 = 100$ kV/cm, $m_z(F_0) = 0.210m_0$ and $A = 2.21 \times 10^{-8}$ cm/V. These coefficients have been derived for a device with a uniform doping profile of 5.0×10^{16} cm^{-3}. In principle they depend on the channel doping and on its profile, however, for most of our purposes, a constant m_z value of $0.215m_0$ has proven to be accurate enough and both the field and the doping dependences have been neglected.

The effective mass for the density of states, m^*, has been derived from

$$\frac{\displaystyle\int g(E) f_p(E)\, dE}{\displaystyle\int f_p(E)\, dE} = \frac{g_\nu m^*}{\pi\hbar^2} \tag{4}$$

where the left hand side is the density of states occupied by holes. The function $g(E)$ is the density of states calculated by following the linear tetrahedron method [7] which provides a detailed integration over the two-dimensional (2-D) Brillouin zone, and $f_p(E)$ is the hole occupation probability function. The right hand side is instead the density of states for a parabolic band with an equivalent effective mass m^* and g_ν is the band degeneracy.

Fig. 1 shows the density of states of the first subband obtained with self-consistent $\mathbf{k}\cdot\mathbf{p}$ calculations at different values of the transverse field. Despite the band is not parabolic and dependent on bias, the effective mass values derived from (4) are always close to $1.15m_0$. The corresponding value of the hole density of states is highlighted by the dashed line in Fig. 1.Fig. 2 shows instead the density of states of the light-holes. It rises less sharply and displays a knee just above the band-edge. This feature depends on the transverse field and cannot be neglected since, at 77 K, the second subband is barely populated and most of the light-holes lie precisely in this energy region. Equation (4) gives an equivalent light-hole density of states effective mass of $0.4m_0$. The dashed line shows the resulting equivalent density of states, which lies below the peak value and closer to the knee near the band-edge.

In summary, at 77 K the hole quantization/density of states effective masses can be taken equal to $0.275m_0/1.15m_0$ for the heavy-holes and $0.215m_0/0.4m_0$ for the light-holes and their dependence on the electric field can be neglected.

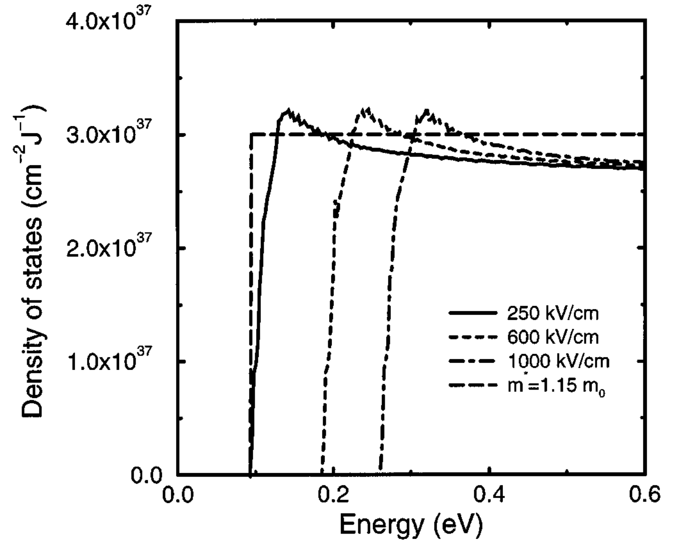

Fig. 1. Density of states for the heavy-hole subband, numerically computed at different values of the effective electric field orthogonal to the Si/SiO$_2$ interface. The dashed line shows the density of states derived in the effective mass approximation with $m^* = 1.15m_0$.

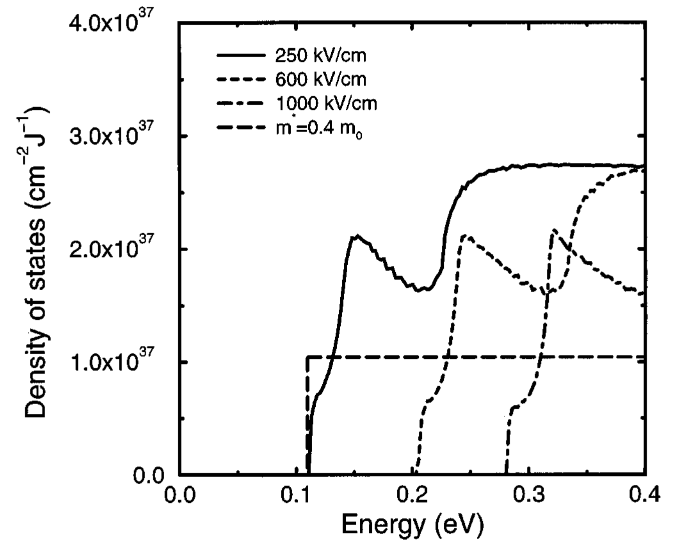

Fig. 2. Density of states of the light-holes numerically computed at different effective electric fields. The dashed line shows the effective density of states computed in the effective mass approximation according to (4). The presence of a knee near the band-edge reduces the effective density of states populated by the light-holes in the bias range of interest.

Fig. 3 finally compares the fractional subband occupancy at 77 K as computed by the $\mathbf{k}\cdot\mathbf{p}$ self-consistent solver with the results of a Schrödinger-Poisson solver [8] using the effective mass values derived above. The device has a channel doping of 5.0×10^{16} cm^{-3}. The results are close, within 1% over the entire range, up to a carrier density N_s of 1.5×10^{13} cm^{-2}. Note that most of the carriers lie in the first subband, thus suggesting that a single subband approximation can be safely adopted in the evaluation of the hole transport properties at 77 K.

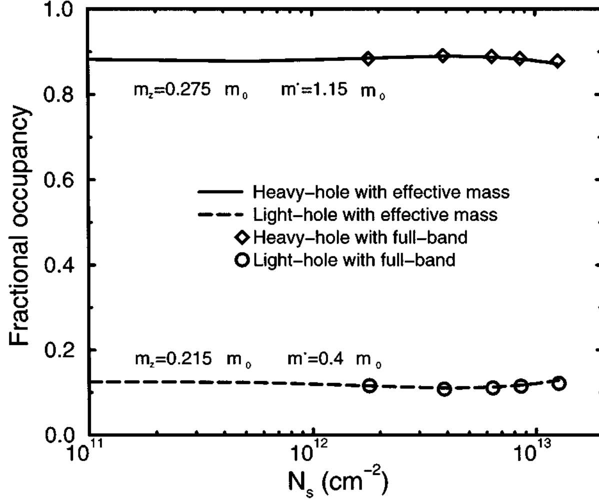

Fig. 3. Fractional occupancy at 77 K in the heavy-hole and light-hole subbands as obtained from the $\mathbf{k}\cdot\mathbf{p}$ procedure and from the effective mass approximation. Note that almost all the carriers lie in the heavy-hole subband.

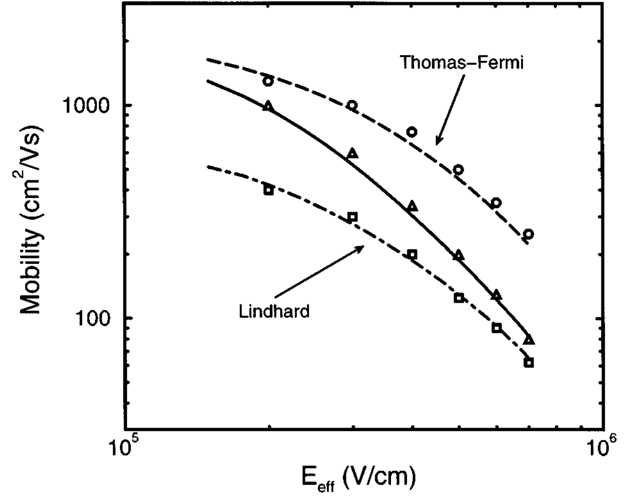

Fig. 4. Effective mobility computed at 77 K by the full-band Monte Carlo procedure (symbols) and based on the relaxation-time approximation (lines). The three data sets refer to different descriptions of the carrier screening: (dashed line) simple Thomas-Fermi approximation; (solid line) carrier screening accounted for by (8); (dot-dashed line) Lindhard's approximation.

III. Surface Roughness Mobility

Surface roughness scattering has been deeply investigated in the past and the reference theoretical framework is reviewed in [6]. In this model, the surface roughness scattering between an initial state with wave-vector k and a final state k' is computed on the basis of the Fermi Golden Rule and is proportional to the matrix element

$$|V_{SR}(q)|^2 = \frac{S(q)\Gamma^2(q)}{\epsilon_r^2(q)} \tag{5}$$

where $q = |k - k'|$ is the wave-vector exchanged in the scattering event, $S(q)$ is the spectral density of the surface roughness, $\Gamma(q)$ includes the electrostatic dependence on the square of the average electric field pushing the carriers against the Si/SiO_2 interface, and $\epsilon_r(q)$ is a wave-vector dependent dielectric constant accounting for the screening due to the free hole gas. In the Thomas-Fermi approximation of the potential screening the dielectric constant is written as [9]

$$\epsilon_r(q) = \epsilon_r \cdot \left(1 + \frac{\overline{q}_s^{TF}}{q}\right) \tag{6}$$

where ϵ_r is the dielectric constant, the screening parameter is

$$\overline{q}_s^{TF} = \frac{g_\nu m^* e^2}{2\pi\epsilon_m \hbar^2} \tag{7}$$

and $\epsilon_m = (\epsilon_{si} + \epsilon_{ox})/2$. A better approximation includes the effect of the finite extension of the wave function introducing a wave-vector dependent screening parameter

$$q_s = \overline{q}_s^{TF} G_{00,00}(q) \tag{8}$$

with

$$G_{00,00}(q) = \int_0^\infty dz \int_0^\infty dz' (e^{-q|z-z'|} + \tilde{\epsilon} e^{-q|z+z'|}) |\xi_0(z')|^2 |\xi_0(z)|^2 \tag{9}$$

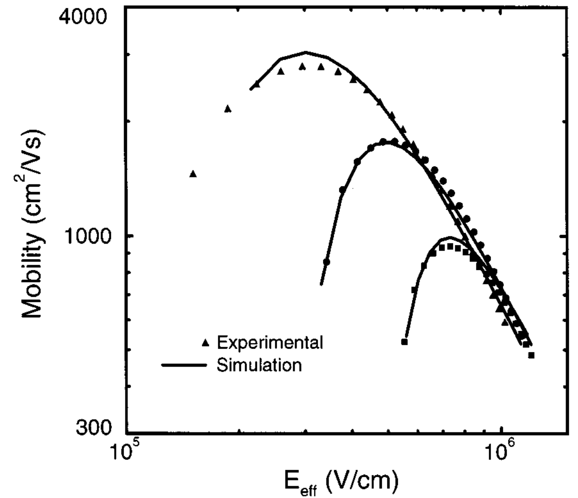

Fig. 5. Comparison between the experimental electron mobility at 77 K and the surface roughness-limited mobility computed using the Gaussian power spectral density in (10) with $\Lambda = 10.3$ Å and $\Delta = 2.7$ Å

where $\tilde{\epsilon} = (\epsilon_{si} - \epsilon_{ox})/(\epsilon_{si} + \epsilon_{ox})$ and $\xi_0(z)$ is the eigenfunction of the lowest state.

Fig. 4 shows a comparison between the mobility computed by the full-band Monte Carlo (symbols) and the results obtained in the relaxation-time approximation by assuming that all the holes lie in the heavy-hole subband with $m^* = 1.15 m_0$ (lines). In all the calculations the surface roughness was described by the power spectral density

$$S(q) = \pi\Lambda^2\Delta^2 e^{-((\Lambda q)^2/4)} \tag{10}$$

taking $\Lambda = 10.3\ A$ and $\Delta = 2.7\ A$. It will be seen in the following that these values make it possible to fit the experimental electron mobility at 77 K (Fig. 5).

The three data sets in Fig. 4 refer to different carrier screening models, namely the simple Thomas–Fermi approximation of (6) (dashed line), the Thomas–Fermi screening with the corrections

given by (8) and (9) (solid line) and the Lindhard's random phase approximation (RPA) [10] (dot-dashed line). In this latter case the $\overline{q}_s^{TF}$ in (8) is replaced with

$$\tilde{q}_s^{TF} = \frac{e^2}{4\pi\epsilon_m} \frac{m^* g_\nu}{\hbar^2} \int_0^1 \frac{f_0\left(bx - \dfrac{E_F}{k_B T}\right)}{\sqrt{1-x}}\, dx \qquad (11)$$

where $b = (\hbar^2 q^2)/(8m^* k_B T)$ and f_0 is the usual Fermi function [11], [12].

The close agreement between the results of the Monte Carlo code (symbols) and those derived in the relaxation-time approximation (lines), independently of the carrier screening model, highlights that both the anisotropy of the valence band structure and its variation with the transverse effective field have a negligible impact on the hole mobility and cannot be responsible for its peculiar dependences. The agreement also demonstrates that the relaxation-time framework is quantitatively reliable and it was therefore extensively used in the following investigation in place of the more computationally expensive Monte Carlo code. Regarding the screening model, note how the simplest Thomas–Fermi screening leads to mobility values four times larger than the Lindhard's approximation. In all the calculations presented in the following Sections we have therefore used the more refined Lindhard's model.

IV. Role of the Power Spectral Density

The power spectral density $S(q)$ accounts for the interface morphology and is defined as the Fourier transform of the auto-covariance function of the surface roughness. A Gaussian auto-covariance function was first proposed [13] leading to the power spectral density of (10). Further experimental investigations [14] suggested that the auto-covariance function may have an exponential shape, corresponding to the power spectral density

$$S(q) = \pi\Delta^2\Lambda^2 \frac{1}{\left[1 + \left(\dfrac{\Lambda^2 q^2}{2}\right)\right]^{3/2}} \qquad (12)$$

where Δ is the r.m.s. value of the roughness asperities and Λ is the roughness correlation length. In practice, the mobility data can be fitted by using either one of the two spectrum shapes. Fig. 5 shows a comparison between the experimental electron mobility at 77 K [2] and numerical results computed assuming a Gaussian spectral density with $\Lambda = 10.3$ Å and $\Delta = 2.7$ Å [15]. However, the same good fitting can be obtained using an exponential auto-covariance function with a shorter correlation length, $\Lambda = 7.0\ A$, and a larger r.m.s value, $\Delta = 4.0\ A$. A choice between the two spectral shapes cannot be made relying on high resolution TEM and AFM measurements. These techniques have not given so far conclusive results [14], [16] and their capability to measure the interface morphology of a real device down to a resolution of the single atomic step, avoiding modifications of the surface quality due to the sample preparation, is still an open issue. Moreover, even if the surface roughness were carefully measured, these results cannot be directly taken as representative of the perturbation potential felt by the carriers moving close to the interface. The microscopy techniques measure the surface morphology and are not able to sense the surface potential which instead enters into the scattering calculations. The latter is expected to be dependent on aspects like the thickness of the non-stechiometric layer between the Si surface and the bulk SiO_2, that cannot be certainly addressed by TEM or AFM measurements.

We have therefore resorted to another approach: take the power spectral density as a description of the potential perturbing the carrier transport and try to derive the $S(q)$ shape. Since the Si/SiO_2 interface of n and p-MOSFET's is expected to be similar, we have required that the $S(q)$ of choice must account for both the electron and the hole mobility data. This requirement is not satisfied neither by the Gaussian nor by the exponential auto-covariance function. Fig. 6 shows the comparison between the experimental hole mobility and the numerical values obtained for devices with different channel doping, using the Gaussian $S(q)$ with $\Lambda = 10.3\ A$ and $\Delta = 2.7\ A$, which can accounts for the electron mobility. Note that the curves do not follow the experimental results. Moreover they do not show a universal behavior, as they do not merge into a single curve when plotted as a function of the effective field with $\eta = 1/3$. However, if the spectrum parameters are changed to $\Lambda = 20.5\ A$ and $\Delta = 1.9\ A$ a more satisfactory agreement can be achieved (dashed lines in Fig. 6). This result highlights that the peculiarities of the hole mobility (i.e., its universality as a function of E_{eff} with $\eta = 1/3$ and the power law degradation as E_{Eff}^{-1}) are linked to the spectrum shape and not to other aspects of the valence band physics. The point is now to derive a new $S(q)$ function.

V. New Shape of the Power Spectrum

The effect of the shape of the power spectral density on the hole and electron mobilities can be satisfactorily discussed in the single-subband relaxation-time approximation. Within this framework, the mobility is computed as [17]

$$\mu_{eff} = \frac{e\langle\tau_m\rangle}{m^*} \qquad (13)$$

where m^* is the density of state effective mass and the momentum relaxation time is given by

$$\frac{1}{\tau_m(E(k))} = \frac{2\pi}{\hbar} \sum_{q=|k'-k|} |V_{SR}(q)|^2 (1 - \cos\theta_{kk'}) \cdot \delta(E(k) - E(k')). \qquad (14)$$

The $\langle\tau_m\rangle$ value is then derived by averaging the above equation over the populated states. At low temperature the average procedure leads to a value close to the momentum relaxation time at the Fermi energy, $\tau_m(k_F)$. We may therefore write

$$\frac{1}{\tau_m(k_F)} \propto E_{av}^2 \int_0^{2\pi} S\left(k_F\sqrt{2(1-\cos\theta)}\right) \cdot (1 - \cos\theta)\, d\theta \qquad (15)$$

where k_F is the carrier wave-vector at the Fermi energy and E_{av} corresponds to the effective field E_{eff} with $\eta = 1/2$, that is the effective field for electrons. It is also worth noting that

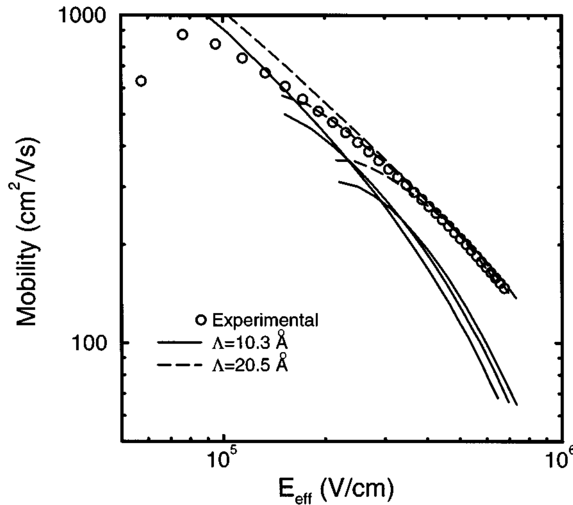

Fig. 6. Comparison between simulated and experimental hole mobilities at 77 K. The solid lines represent the hole mobility computed for devices at different channel doping by using the Gaussian power spectral density in (10) with $\Lambda = 10.3$ Åand $\Delta = 2.7$. ÅThe dashed lines, closer to the experimental data, have been instead obtained by using $\Lambda = 20.5$ Å and $\Delta = 1.9$. Å

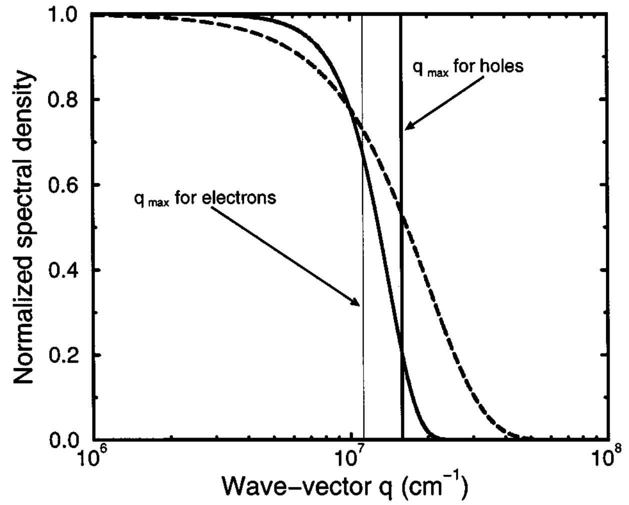

Fig. 7. Power spectral density shape given by (17) (solid line) compared with the shape of a Gaussian power spectral density (dashed line) with the same parameters. The vertical straight lines are the highest spatial components ($q_{\max}$) affecting the surface roughness-limited mobility of electrons and holes computed at a carrier concentration of 10^{13} cm^{-2}.

the main contribution to the integral in (15) is the one for $\theta = \pi$ and corresponds to the spatial frequencies of the roughness spectrum close to $q_{\max} = 2k_F$. At low temperature the carrier wave-vector at the Fermi energy is given by

$$k_F = \sqrt{\frac{2\pi N_s}{g_\nu}} \tag{16}$$

which is dependent on the carrier concentration N_s and on the band degeneracy, but it is independent of the effective mass value. Therefore at a given N_s the twofold degeneracy of the electron subband leads to a k_F value $\sqrt{2}$ lower than that of the holes. This difference remains even if the anisotropy of the valence band is taken into account. It follows that the range of the q components contributing to the hole surface roughness-limited mobility is wider, thus making the hole transport more sensitive to the high-frequency tail of the roughness power spectrum. Fig. 7 shows the Gaussian $S(q)$ accounting for the experimental values of the electron mobility (dashed line). The vertical straight lines in Fig. 7 represent the $q_{\max} = 2k_F$ for electrons and holes at $N_s = 10^{13}$ cm^{-2}.

The bias dependence of the electron and hole surface roughness-limited mobilities can be qualitatively explained referring to Fig. 7 and (15): As the bias increases, both the carrier density and k_F increase. If the intensity of the power spectral density remains almost constant over the range spanned by k_F, the mobility decreases as E_{av}^{-2} [see (15)]. This is the case for electrons. The Gaussian $S(q)$ accounting for their experimental mobility is in fact almost constant in the low-q range (Fig. 7). By using the same Gaussian spectrum (Fig. 6) to compute the hole mobility an effective field dependence weaker than E_{av}^{-2} is obtained, even if it is not sufficient to fit the experimental data yet. This is due to the higher k_F values reached by the holes, which make the integral in (15) decreasing with $S(q)$. This analysis highlights that in order to account for both the hole and the electron mobility data $S(q)$ has to be similar to the Gaussian shape in the low q-region (thus making possible to fit the electron mobility), but with a steeper decay at high q-values to follow the weaker effective field dependence of the hole mobility. A simple function that meets such requirements is

$$S(q) = \pi\Lambda^2\Delta^2 e^{-((\Lambda q)^4/4)} \tag{17}$$

Taking again $\Lambda = 10.3$ A and $\Delta = 2.7$ A both the electron and hole mobility data can be successfully fitted. Fig. 8 shows the hole surface roughness-limited mobility computed with the new power spectral density and plotted as a function of E_{eff} with $\eta = 1/3$. The curves have been derived in the relaxation-time approximation, including Lindhard's screening. The values at some bias points have also been checked with the full-band Monte Carlo. Note that even if the channel doping changes from 10^{16} cm^{-3} to 5.0×10^{17} cm^{-3} all the curves approach the same universal dependence with a slope close to E_{eff}^{-1}. The figure also shows for reference the curves computed by using the Gaussian $S(q)$.

Fig. 9 shows the comparison between the experimental data and the mobility values computed for electrons and holes by using the power spectral density (17) with $\Lambda = 10.3$ A and $\Delta = 2.7$ A. Note that the electron mobility is still in close agreement with the experimental data, while the adoption of the new power spectral density (17) makes possible to fit very well the hole data without changing any spectrum parameter.

It may be interesting to compare the difference between the spatial dependence of the roughness described by the spectra presented in [14] and in this section, namely a Gaussian, an exponential and the new $S(q)$ given by (17). Fig. 10 shows typical samples of the roughness described by these spectra. The dots in the same figure show as a reference the lattice sites of the Si⟨111⟩ fringes at the Si⟨100⟩ surface. The spatial pattern has been generated by adding a random phase to each spectral component in the Fourier domain and then inverse-transforming. Note how similar are the spatial features of the Gaussian surface and of the surface described by the new spectrum. Both of them are quite compatible with the typical lattice distance at the

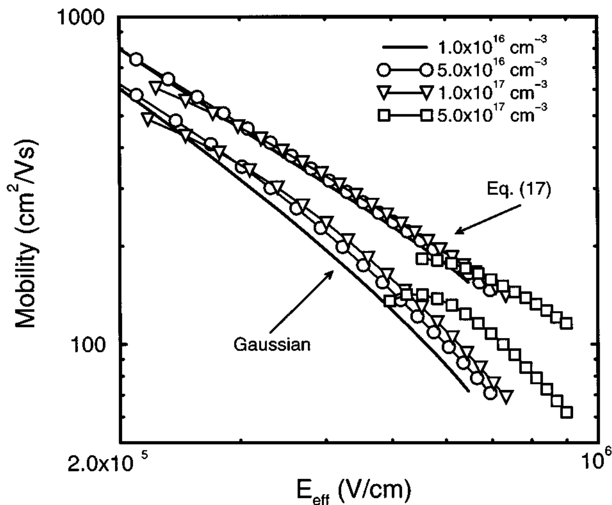

Fig. 8. Hole surface roughness-limited mobility at 77 K computed with a Gaussian power spectral density and with the spectrum shape given by (17). In both cases $\Lambda = 10.3$ Å and $\Delta = 2.7$. ÅThe cures are plotted as a function of the effective electric field with $\eta = 1/3$.

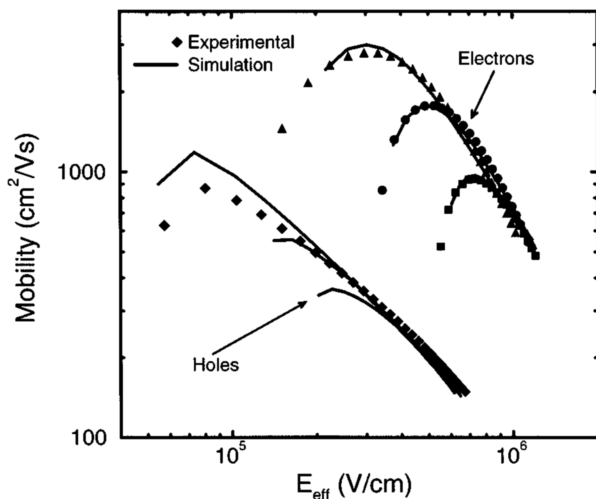

Fig. 9. Experimental values of the effective mobility of electrons and holes at 77 K (symbols) plotted as a function of the effective field with $\eta = 1/2$ and $\eta = 1/3$,, respectively. The solid lines are the effective mobility computed by using the power spectral density in (17).

interface. On the contrary, the surface described by the exponential model (adopting the same Λ and Δ values), shows spikes on distances shorter than the lattice steps. It is quite unlikely that the potential perturbing the carrier motion at the interface can feature such a high-frequency components.

VI. Conclusion

In this work, we have investigated the dependences of the surface limited mobility of the holes at 77 K and its differences with respect to the electron mobility. Based on Monte Carlo simulations and on an equivalent relaxation-time numerical model, we have shown that the peculiar features of the hole mobility are due neither to the valence band anisotropy nor to its dependence on the external bias. The hole mobility can be instead accounted for properly if the shape of the surface roughness power

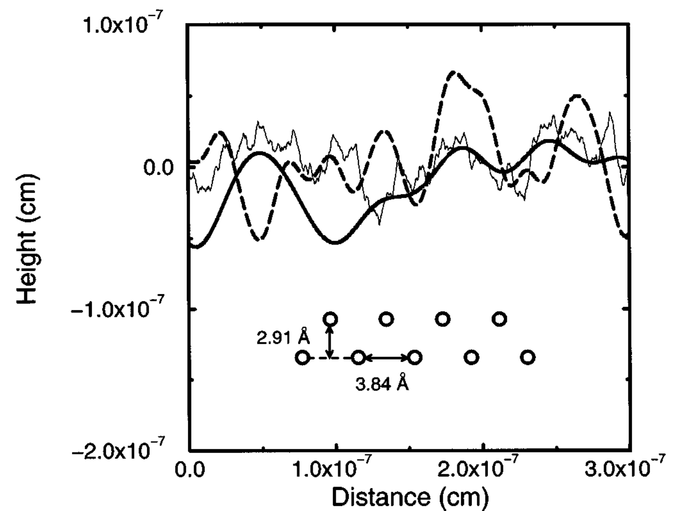

Fig. 10. One-dimensional random surface generated from the modified Gaussian model (17) (solid line) compared with the surfaces generated from a Gaussian (dashed line) and an exponential model (thin solid line). All the three surfaces have been generated by using $\Delta = 0.27$ Å and $\Lambda = 10.3$. Å The circles point out the relevant dimensions of lattice steps.

spectrum is slightly changed with respect to the shapes corresponding to Gaussian or exponential auto-covariance functions so far adopted in the literature. We have identified a new spectrum shape that makes possible to account for the experimental dependences of both the electron and the hole mobilities, with the same set of parameters. We have also shown that the spatial features of the roughness described by this latter $S(q)$ are very close to those described by a Gaussian power spectrum.

Acknowledgment

Prof. P. Vogl is gratefully acknowledged for his support and encouragement of this research project.

References

[1] A. G. Sabnis and J. T. Clemens, “Characterization of teh electron mobility in the inverted $\langle 100 \rangle$ Si surface,” in *IEDM Tech. Dig.*, 1979, pp. 18–21.

[2] S. Takagi, A. Toriumi, M. Iwase, and H. Tango, “On the universality of inversion layer mobility in Si MOSFET’s: Part I—Effects of substrate doping concentration,” *IEEE Trans. Electron Devices*, vol. 41, pp. 2357–2362, Dec. 1994.

[3] S. Jallepalli *et al.*, “Understanding the differences in the effective-field dependence of electron and hole inversion layer mobilities,” in *IEDM Tech. Dig.*, 1996, pp. 391–394.

[4] R. Oberhuber, G. Zandler, and P. Vogl, “Subband structure and mobility of two-dimensional holes in strained Si/SiGe MOSFETs,” *Phys. Rev. B*, vol. 58, pp. 9941–9948, Oct. 1998.

[5] Y. X. Liu, D. Z.-Y. Ting, and T. C. McGill, “Efficient, numerically stable multiband $k \cdot p$ treatment of quantum transport in semiconductor heterostructures,” *Phys. Rev. B*, vol. 54, pp. 5675–5683, Aug. 1996.

[6] T. Ando, A. B. Fowler, and F. Stern, “Electronic properties of two-dimensional systems,” *Rev. Mod. Phys.*, vol. 54, pp. 437–672, Apr. 1982.

[7] G. Wiesenekker, G. te Velde, and E. Baerends, “Analytic quadratic integration over the two-dimensional brillouin zone,” *J. Phys. C*, vol. 21, pp. 4263–4283, Aug. 1988.

[8] A. Pacelli, “Self-consistent solution of the Schrödinger equation in semiconductor devices by implicit iteration,” *IEEE Trans. Electron Devices*, vol. 44, pp. 1169–1171, July 1997.

[9] F. Stern and W. E. Howard, “Properties of semiconductor surface inversion layers in the electric quantum limit,” *Phys. Rev.*, vol. 163, pp. 816–835, Nov. 1967.

[10] J. Lindhard, “Kgl. danske videnskab, selskab,” *Mat.-Fys. Medd.*, vol. 28, no. 8, 1954.
[11] F. Stern, “Polarizability of a two dimensional electron gas,” *Phys. Rev. Lett.*, vol. 18, pp. 546–548, Apr. 1967.
[12] M. V. Fischetti and S. E. Laux, “Monte Carlo study of electron transport in silicon inversion layers,” *Phys. Rev. B*, vol. 48, pp. 2244–2273, July 1993.
[13] R. E. Prange and T. W. Nee, “Quantum spectroscopy of the low-field oscillations in the surface impedance,” *Phys. Rev.*, vol. 168, pp. 779–786, Apr. 1968.
[14] S. M. Goodnick *et al.*, *Phys. Rev. B*, vol. 32, pp. 8171–8186, Dec. 1985.
[15] G. Mazzoni, A. L. Lacaita, L. M. Perron, and A. Pirovano, “A detailed study of electron mobility degradation by surface scattering in ULSI MOSFET’s,” in *Proc. ESSDERC’98*, pp. 328–331.
[16] T. Yamanaka *et al.*, “Correlation between inversion layer mobility and surface roughness measured by AFM,” *IEEE Trans. Electron Devices*, vol. 17, pp. 178–180, Apr. 1996.
[17] G. Mazzoni, A. L. Lacaita, L. M. Perron, and A. Pirovano, “On surface roughness-limited mobility in highly doped n-MOSFET’s,” *IEEE Trans. Electron Devices*, vol. 46, pp. 1423–1428, July 1999.

Agostino Pirovano (S’98) was born in Italy in 1973. He received the Laurea degree in electrical engineering from the Politecnico di Milano, Milan, Italy, in 1997. Currently, he is pursuing the Ph.D. degree in the Department of Electrical Engineering Politecnico di Milano, working in the silicon device and technology area.

His research interests include the modeling and characterization of transport properties in MOS devices and the physics of Si/SiO_2 interface.

Andrea L. Lacaita (M’90–SM’94) was born in 1962 in Manduria, Italy. He received the Laurea degree in nuclear engineering in 1985 from the Politecnico of Milano, Milan, Italy.

In 1987, he joined the Italian National Research Council as a Researcher. In 1990, he was a Visiting Scientist at the AT&T Bell Laboratories, Murray Hill, NJ, where he worked on the photorefractive effects in super lattices. In 1992, he was appointed Associate Professor of Electronics at the Politecnico of Milano. His current research interests are physics of carrier transport in semiconductor devices, development of new experimental methods for characterization of semiconductor material and devices, and low noise design of integrated circuits for cellular recrivers.

Günther Zandler received the Ph.D. degree from the University of Innsbruck, Austria, in 1989.

In 1988, he became a Research Associate at the Institute for Experimental Physics, University of Innsbruck. In 1989, he joined the Physics Department of the Technical University of Munich as Research Associate for theoretical semiconductor physics. His research interests focuses on the physics and simulation of electron devices, high field transport, and ultrafast phenomena in bulk and nano-structured semiconductors. Further, he is engaged in the development of efficient numerical techniques for particle based simulators.

Ralph Oberhuber received the M.S. degree in physics from the Technical University of Munich, Munich, Germany, in 1996, and the Ph.D.degree in solid state physics in 1998. His research field covered SiGe MOSFET’s, AlGaN heterostructures, and quantum devices.

In November 1998, he joined the Mixed Signal and Logic Products Department of Texas Instruments Deutschland GmbH, Freising, Germany. Since then, he works on CMOS chip design for transponder systems.

Dr. Oberhuber has a U.S. patent pending on analog circuit design.